Bull Volcanol (2015) 77: 96
DOI 10.1007/s00445-015-0981-4

RESEARCH ARTICLE

Influence of slope angle on pore pressure generation and kinematics of pyroclastic flows: insights from laboratory experiments

Corentin Chédeville[1] · **Olivier Roche**[1]

Received: 24 March 2015 / Accepted: 13 October 2015 / Published online: 19 October 2015

Abstract The influence of slope angle on pore pressure generation and kinematics of fines-rich pyroclastic flows was investigated through laboratory experiments. Granular flows were generated by the release of a column of fine glass beads (d=0.08 mm) in an inclined channel (0–30°). The granular column could be fluidized while the channel base was either smooth or made rough by glued beads of 3 mm diameter. Pore pressure measurements reveal that the degree of autofluidization, caused by air escaping from the substrate interstices into which flow particles settled, was high at all slope angles. Flow runout increase due to autofluidization, however, was reduced at slope angle higher than ~12° because of the occurrence of a strong deceleration phase that limited the flow duration. This is probably caused by the combination of flow head thinning at increased slope angle and settling of particles into the substrate interstices until the flow ran out of mass. Analysis of high-speed videos suggests that ingestion of ambient air at the flow front did not occur, even on steep slopes of 30°. Experiments at inclinations close to (25°) or slightly higher (30°) than the repose angle of the granular material (28.5°) revealed the formation of a thin basal deposit that was then eroded as the flow thickness and velocity gradually decreased. Our study suggests that air escape from substrate interstices in nature can be a significant external cause of pore pressure generation that favors low energy dissipation and long runout distances of pyroclastic flows on moderate topographies.

Keywords Pyroclastic flows · Fluidization · Pore pressure · Analog modelling · Inclined substrate · Substrate roughness

Editorial responsibility: G. Lube

✉ Corentin Chédeville
c.chedeville@opgc.univ-bpclermont.fr

[1] Laboratoire Magmas et Volcans, Université Blaise Pascal, CNRS, IRD, OPGC, 5 rue Kessler, 63038 Clermont-Ferrand, France

Introduction

Pyroclastic density currents are common in nature and can be a major threat for populations as they are hot, fast, challenging to predict, and have runout distances that can exceed 100 km (Valentine et al. 1989; Wilson et al. 1995; Druitt 1998; Branney and Kokelaar 2002). Their dynamics can vary significantly depending on their triggering mechanism (eruption column or dome collapse, boiling over, lateral explosion), volume, granulometry, sorting (Sparks 1976; Wilson 1980; Druitt et al. 2007), and topography (Fisher et al. 1993; Woods et al. 1998; Lube et al. 2007) as well as the nature of the substrate on which they propagate (Wilson 1980; Roche et al. 2013; Chédeville and Roche 2014). The present study addresses the dynamics of pyroclastic density currents with a concentrated basal part, referred to as "pyroclastic flows" hereafter.

Pyroclastic flows propagate on slopes that range from more than 30° near the summits of volcanoes down to ~0° at more distal areas. Several field studies have addressed the influence of the slope angle on their deposition, segregation, and erosion mechanisms (Sparks et al. 1997; Giordano 1998; Calder et al. 2000; Lube et al. 2007; Bernard et al. 2014; Brand et al. 2014). Further insights were gained from analog and numerical modelling of granular flows down inclined substrates that revealed fundamental aspects of flow dynamics (e.g., GDR MiDi 2004; Mangeney et al. 2007). Recent experimental works, in particular, have investigated the influence of a rough

erodible or rigid granular substrate on flow velocity and runout distance (Mangeney et al. 2010; Lube et al. 2011; Farin et al. 2014). These studies, however, involved flows of particles larger than 0.1–1 mm for which the influence of the interstitial gas (air) is negligible, in contrast to fines-rich pyroclastic flows (Roche et al. 2006; Druitt et al. 2007; Girolami et al. 2008; Rowley et al. 2014). Here, we define fines-rich flows as concentrated granular mixtures with a high (typically >50 wt.%) proportion of ash and a low hydraulic permeability. Analog experiments involving fine particles (<0.1 mm) have demonstrated that low material permeability greatly reduces diffusion of the gas pore pressure from within the granular mixture, which favors flow propagation and increases runout distances compared to equivalent but non-fluidized flows (e.g., Roche 2012). These flows of fine particles consisted of a sliding (i.e., non zero velocity at the base) head that generated relative underpressure that scaled with the square of the front velocity (Roche et al. 2013) while the flow body behind the head generated overpressure when pore pressure was provided at source (Roche et al. 2010; Roche 2012). Recently, Chédeville and Roche (2014) showed that flows of such fine particles without initial pore pressure and propagating on a horizontal rough, rigid substrate could be autofluidized as particles settled into the substrate interstices, which caused an upward flux of air that generated pore pressure in the granular mixture. The present study aims at extending the work of Chédeville and Roche (2014) by investigating the influence of the slope angle on the autofluidization mechanism evidenced by their experiments. We report data on gas pore pressure at the flow base, flow runout distance, and front kinematics as a function of the slope angle, varying from horizontal to 30°.

Experimental methods

Pore fluid pressure generation and diffusion in gas-particle systems

Pore fluid pressure in a bed of particles can be generated when there is a relative vertical motion between the gas moving upward and the particles settling downward. The gas exerts a drag force that increases with its velocity, which counterbalances the weight of the particles and reduces the interparticle frictional forces (Rhodes 1998). The bed is said to be fluidized when the drag force equals the apparent weight of the particles, which occurs at superficial gas velocity called the minimum fluidization velocity (U_{mf}). This minimum velocity increases with particle size and density, meaning that it is easier to fluidize beds of small and light particles.

Once generated, the interstitial pore fluid pressure does not vanish instantaneously even if there is no more relative gas-particle motion. The pore pressure decreases through diffusion according to

$$\frac{\partial P}{\partial t} = D\frac{\partial^2 P}{\partial z^2} \quad (1)$$

where P is the pore pressure, z is the bed height, t is the time, and D is the hydraulic diffusion coefficient (Iverson 1997). D is proportional to $k/(1-\varepsilon_s)\mu\beta$, with k the bed hydraulic permeability, ε_s the particle volume fraction, μ the gas dynamic viscosity, and β the gas compressibility. The pressure diffusion timescale of a bed of thickness H increases proportionally to H^2/D (Iverson 1997; Montserrat et al. 2012; Roche 2012). At a laboratory scale, pore pressure diffuses almost instantaneously (<<1 s) in beds of particles typically larger than 100 μm, with permeability $k>10^{-10}$ m^2. In contrast, the low permeability $k<10^{-10}$ m^2 of beds of finer particles (e.g., the matrix of fines-rich ignimbrites) allows diffusion for longer durations, which can be up to several minutes or even hours when scaled to the natural system (Druitt et al. 2007; Montserrat et al. 2012; Roche 2012).

Experimental device and procedure

Dam break experiments were carried out in the same apparatus as the one used by Chédeville and Roche (2014). The device consisted of a 20×10 cm reservoir connected to a 300×10 cm tilting channel in which flows were generated (Fig. 1). Opening of the reservoir gate by means of a counterweight was fast enough to have a negligible influence on the spreading of the granular material from the reservoir. The flow particles were sub-spherical glass beads of mean diameter d= 0.08 mm and with a density of 2500 kg m^{-3}. To avoid possible cohesion effects caused by ambient moisture, we fluidized the particles with dry air in a fluidization rig for at least 10 min before each experiment. For some experiments, a gas flux was provided at the base of the reservoir through a porous plate in order to fluidize the particles (i.e., generate pore pressure) before they were released in the channel. The superficial gas velocity was set above the minimum bubbling velocity (U_{mb}) of beds of fine particles (~13–16 mm s^{-1}>U_{mf}) so that full bed support was achieved and bed expansion (~7–8 %) was maximal. No gas flux was provided from the channel base in any experiment. The mass of particles initially placed in the reservoir was set to 3, 6, or 12±0.001 kg, which corresponded to column heights of about 10, 20, and 40 cm, respectively. The channel base was either smooth or covered by a layer of glued glass beads with a mean diameter d=3.0±0.1 mm in order to form a rough non-erodible substrate (see Chédeville and Roche (2014) for details). The choice of using a 3-mm rough bed was motivated by the fact that this roughness had the strongest influence on the runout of horizontal flows (Chédeville and Roche 2014). Moreover, complementary experiments with lower roughness (d=0.7±0.1 mm) showed

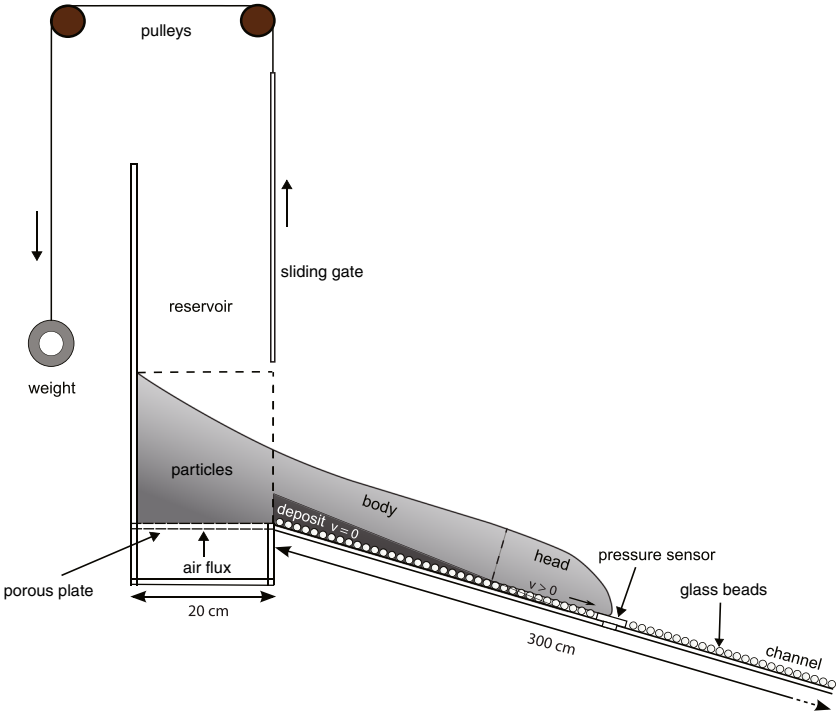

Fig. 1 Experimental device consisting of a (fluidization) reservoir connected to a 3-m-long inclinable channel whose base is either smooth or made rough by gluing 3-mm glass beads. When the gate opens, the spreading of the column of particles generates a flow consisting of a sliding head followed by a body at base of which forms and aggrading deposit

that the flows generated low pore pressure signals difficult to analyze (see in the "Results" section).

The channel was inclined at slope angles ranging from 0 to 30°, the latter being larger than the repose angle of the flow particles (28.5±1°), while the reservoir base was always horizontal. The flows generated had typical thicknesses of 0.5–6 cm and maximum front velocities of 0.5–5 m/s depending on the initial conditions (i.e., presence or absence of pore pressure in the reservoir, column height, and channel inclination). The experiments were filmed by means of a high-speed video camera (Fastcam SA3) at rates of 250 to 3000 frames/s with corresponding resolutions of 1024×1024 to 896×736 pixels, depending on the portion of the flow investigated. To measure the gas pore pressure within the flow, we used piezoresistive pressure sensors at distances of 10, 50, 90, and 150 cm from the gate. The sensors were covered by a 36-μm grid to prevent any contact with the particles and were placed at the same level as the top of the glued beads (Chédeville and Roche 2014, their Fig. 4b).

The experiments were scaled in order to ensure dynamic similarity with fines-rich pyroclastic flows according to the dimensional analysis of Roche (2012) and Chédeville and Roche (2014). Considering same values of the roughness number $R_0=h/D_0$ proposed by Chédeville and Roche (2014) in nature and experiments, with h the flow thickness and D_0 the substrate roughness, and the fact that experimental flows have a thickness h=1–6 cm, then the 3-mm rough substrate used in this study represents a natural roughness of ~0.05–0.3 to ~0.5–3 m for 1-m-thick to 10-m-thick pyroclastic flows, respectively. We thus believe that our experimental configuration represents a wide range of rough terrains that could be commonly observed in natural configurations.

Results

Pore pressure data

Pore pressure data were acquired at five different slope angles (0°, 8°, 16°, 25°, and 30°) for both initially fluidized and non-fluidized flows generated from a column of initial height of 40 cm on both smooth and 3-mm rough substrates. For initially non-fluidized flows on a smooth substrate (Fig. 2), no positive pore pressure was measured at any slope angles investigated except close to the reservoir (10 cm), in some experiments, where small positive pressure (<60 Pa) was recorded as in earlier similar works (Roche et al. 2010). The underpressure phase, caused by the sliding head of the flows, had an amplitude that increased with the slope angle and the distance in the channel while its duration only increased with distance.

For flows propagating on a 3-mm rough substrate (Fig. 3), pore pressure data were normalized with the lithostatic pressure $P_L=\rho_f gh$, with ρ_f the bulk density of the flow (1450±50 kg/m^3), g the gravitational acceleration, and h the flow height above the sensor. The flow height was measured from the position of the flow upper surface along the channel backwall on which a 2×2 cm grid was drawn. Error bars in Fig. 3 correspond to the imprecision on the measurements of the flow thickness and the possible variation of the flow density due to material expansion. The video frame rate was more

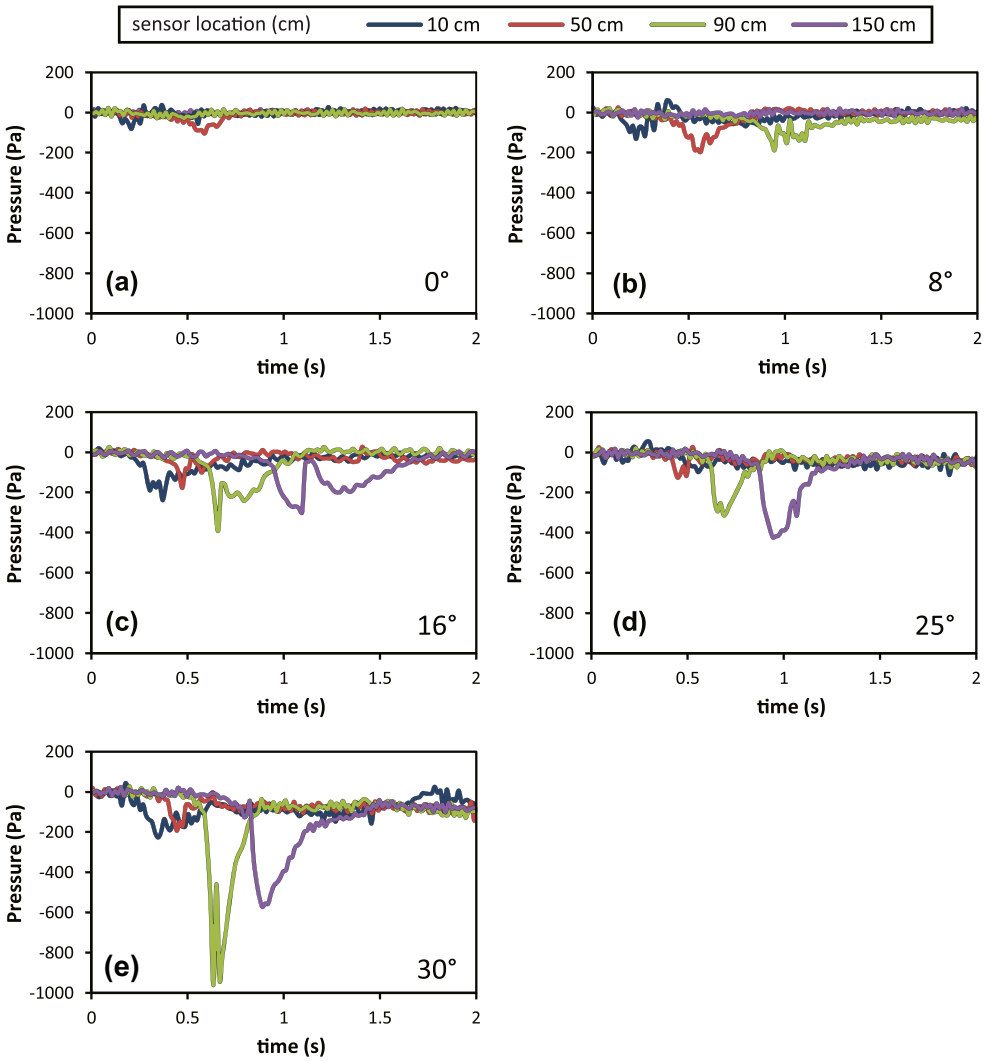

Fig. 2 Basal pore fluid pressure as a function of time after the release of a 40-cm high column of particles from the reservoir, for initially non-fluidized flows over a smooth substrate, at inclinations of **a** 0°, **b** 8°, **c** 16°, **d** 25°, and **e** 30°

than 4 times the sampling rate of the pressure sensors so that each pressure value could be precisely correlated to the instantaneous flow thickness. The normalized pressure accounts for the degree of fluidization for positive pore pressure but is not relevant for the first underpressure phase, which is believed to be a dynamic phenomenon (Roche et al. 2013). Positive pore pressure was measured for both initially fluidized and non-fluidized flows at all slope angles investigated.

For initially non-fluidized flows (Fig. 3a–e), underpressure was generated at the foremost part of the head but was of shorter duration and much lower amplitude (~−100 Pa) than for a smooth substrate (−200 to −500 Pa). Then the flow generated a positive pore pressure that compensated 40–100 % of the lithostatic pressure. The ratio P/P_L >1 measured in some cases can be explained by rapid variation of the flow thickness compared with the timescale of pressure diffusion once pressure was generated (see Roche et al. (2010), their Fig. 12). At a slope angle larger than 8°, the lowest values of the normalized pore pressure (P/P_L ~40–50 %) were measured close (10 cm) to the gate whereas at further distance (50–150 cm), values were significantly higher (P/P_L>70 %). Note that there was no clear dependence of the pressure ratio on the slope angle at a given distance. The flow length (x), corresponding to the duration of the positive pore pressure peak (see below), increased with both the slope angle and the distance in the channel (Fig. 4a). Measurements of x were made either by correlating the peak duration with the flow front position on the video or by multiplying the front velocity by the duration of the overpressure phase if the front overpassed the channel length. Normalizing this length with the total flow length (Fig. 4b, c) shows that a large proportion of the flow was affected by the overpressure, increasing from 20–60 % at the horizontal to 55–90 % at an inclination of 30°. Note that we considered that the length x affected by the overpressure included the foremost part of the flow at base of which underpressure was measured instead (Fig. 4c). In fact, this underpressure is believed to have a dynamical origin and might be limited to the flow-substrate interface, possibly masking overpressure within the flow above (Roche 2012; Roche et al. 2013).

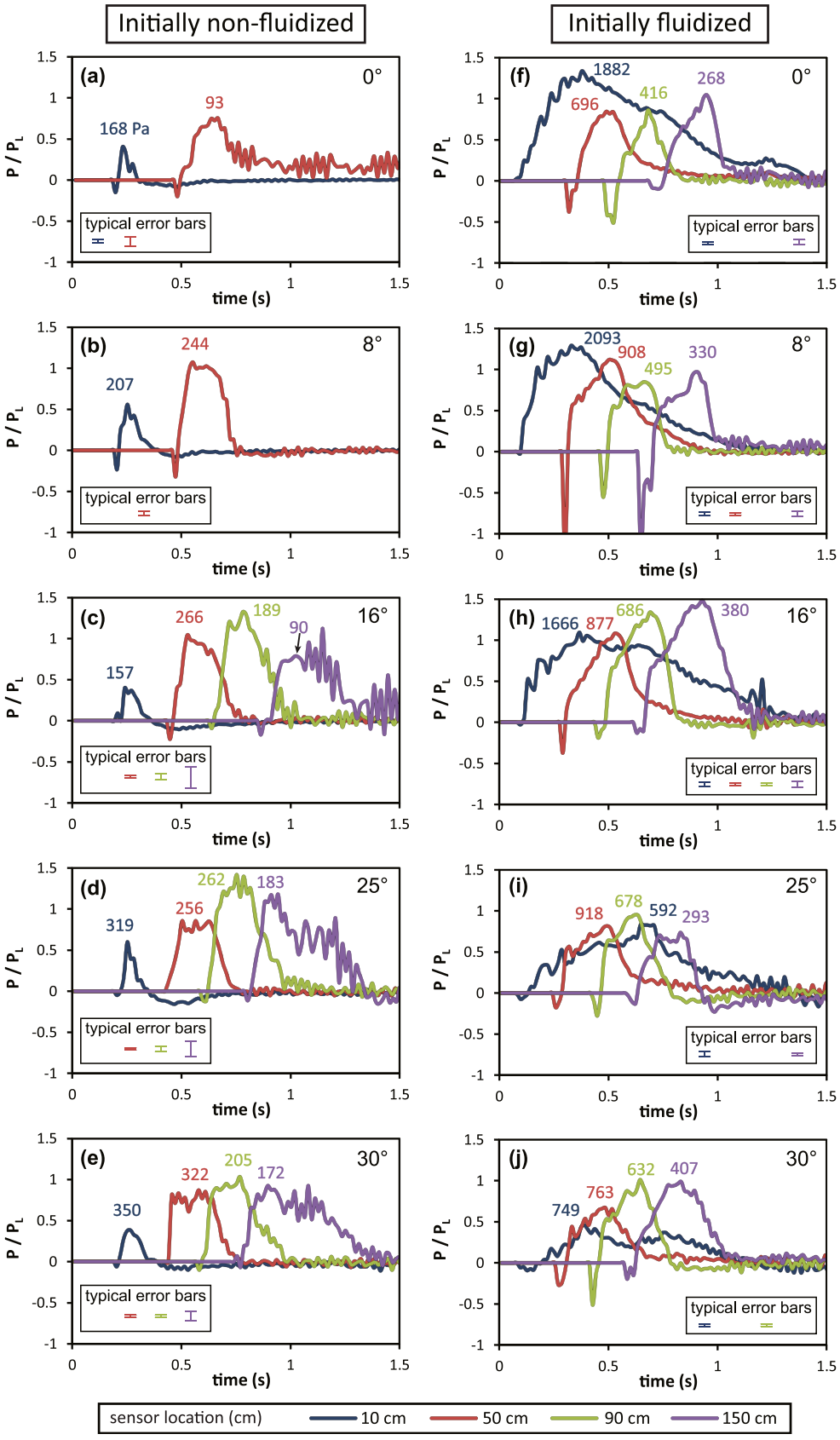

Fig. 3 Basal pore fluid pressure, P, normalized with the lithostatic pressure, P_L, as a function of time for **a**–**e** initially non-fluidized and **f**–**j** initially fluidized flows propagating over a rough substrate. Slope angle was 0–30° and initial column height was 40 cm. High pore pressure fluctuation for some data at 90–150 cm is due to very low flow thicknesses for which the sensor noise becomes non-negligible. Numbers above the curves represent the peak raw pressure values, in Pascal, for each sensor location. Note that these values do not necessarily correspond to the highest raw pressure measured by the sensors. Typical *error bars* are represented for each sensor location with the corresponding color code and account for imprecisions in measurements of the flow thickness and possible variation of bulk flow density due to material expansion of 0–8 %. *Error bars* smaller than the line thickness are not represented. For flows at inclinations of 0 and 8°, positive pore pressure was also measured at distances of 90 and 150 cm from the gate, but *error bars* were so large that we chose to not represent the corresponding curves

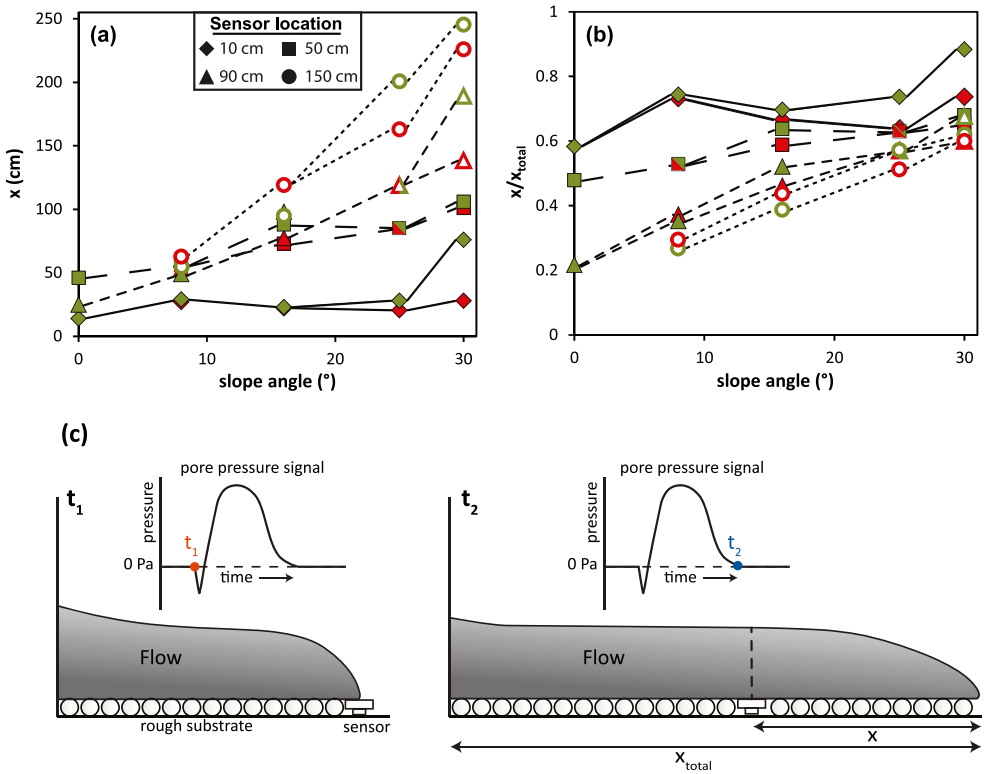

Fig. 4 Initially non-fluidized flows on a rough substrate. **a** Flow length affected by autofluidization (x) as a function of the slope angle, for sensors located at various distances in the channel. **b** Ratio of x over the total flow length (x_{total}) as a function of the slope angle, with same legend as in **a**. The *two colors* represent two experiments for each slope angle investigated. *Closed and open symbols* represent, respectively, x obtained from correlation of the pressure peak duration with the flow front position on the video or from the peak duration times the flow front velocity. The sketch **c** (not to scale) illustrates the relations between the pore pressure signal and the flow location when the front reaches the sensor (t_1) and at the end of the overpressure phase (t_2). Measurements of x and x_{total} reported in **a** and **b** were both taken at time t_2. Note that x also includes the first short underpressure phase at the flow front

In the case of initially fluidized flows over a rough substrate (Fig. 3f–j), the overpressure phase measured close to the reservoir (10 cm) lasted longer than for initially non-fluidized flows while its amplitude decreased with slope angle, from P/P_L~100 % at 0° to P/P_L~40 % at 30°. Further downstream the influence of initial fluidization was not evident as initially non-fluidized flows generated similar pressure signals. There was no clear tendency of the variation of maximum pore pressure value with slope angle.

Results were comparable to those described above for flows propagating over a less rough substrate (d=0.7 mm) except at a long distance from the gate (90–150 cm) for initially non-fluidized flows, where pore pressure signals were too low to be clearly distinguished from the sensor noise as the flows became very thin (<0.2 cm).

Flow runout

Runout distances of flows propagating over smooth or 3-mm rough substrates were measured at slope angles ranging from 0 to 20° with intervals of 2° (Fig. 5). Flow runout could not be measured at higher inclinations as it exceeded the channel length. Experiments were carried out with initial particle column heights of 10 or 20 cm, in both initially fluidized and non-fluidized conditions.

For initially non-fluidized flows propagating on a smooth substrate (Fig. 5a), the flow runout increased with the slope angle and the data defined a trend similar to that reported by Mangeney et al. (2010) and Farin et al. (2014) for flows of larger beads (0.6–0.8 mm). These authors found that

$$\frac{r}{H} = \frac{2\sigma}{\tan\delta - \tan\theta}, \qquad (2)$$

with r as the flow runout, H the initial column height, σ an empirical coefficient that is equal to 0.5 (Mangeney et al. 2010), δ the effective friction angle of the material, and θ the slope angle. For our experiments, the model fitted the data for a friction angle δ=23°, lower than the material repose angle (28.5±1°) but very close to the surface angle of the deposit left in the reservoir (~22±1°). At steeper slope angles, late stage motion of particles at the surface of the deposit once the flow front stopped could cause runout increase by up to 50 % at 20° (see error bars in

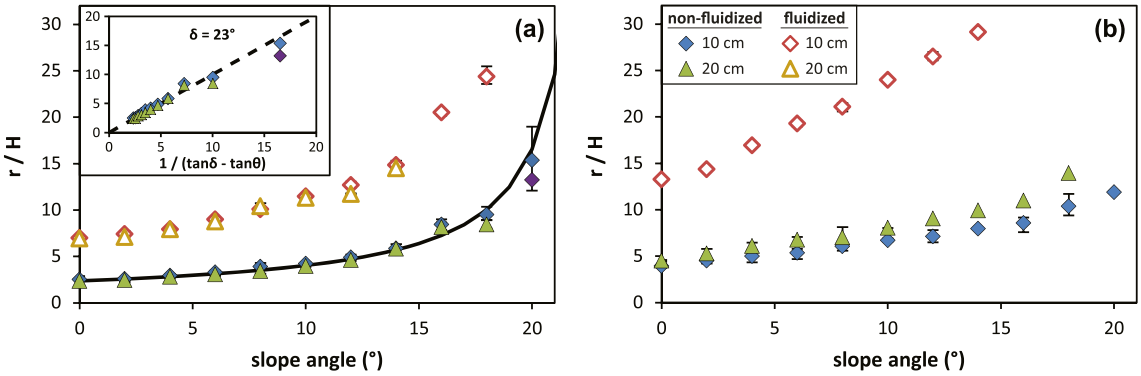

Fig. 5 Flow runout, r, normalized with the initial column height, H, as a function of the slope angle, θ, for **a** a smooth substrate and **b** a 3-mm rough substrate (same legend for both graphs). In **a**, the *solid line* corresponds to the best fit of the runout of non-fluidized flows, obtained using Eq. 2 for a friction angle of δ=23° and the *inset* represents the normalized runout as a function of the rescaled slope angle. The *purple diamond* at 20° corresponds to the flow runout before the front was overtaken by late-stage motion at the upper free surface. *Error bars* represent minimum and maximum runout distances measured for 3–8 repeated experiments and can be smaller than symbols

Fig. 5a). For initially fluidized flows, the friction increased with time as pore pressure diffused. Following Lucas and Mangeney (2007) and Roche et al. (2011), who addressed flows on horizontal slopes, we tried to define a mean effective (reduced) friction angle so that Eq. 2 could fit our data. We did not succeed as we found that the friction angle that best fitted our data at θ=0° was δ=8.5° whereas it was as high as δ=20.1° at an inclination of 18°.

The data for flows over a rough substrate reveal similar trends as observed for a smooth substrate, but with higher normalized runouts at a given slope angle (Fig. 5b). At angles >12°, larger normalized runouts of initially non-fluidized flows for column height H=20 cm compared with H=10 cm could be caused by a larger initial volume of material in the reservoir (Farin et al. 2014). As for fluidized flows over a smooth substrate, we were not able to fit the data with inclination using a mean effective friction angle. Note that for slope angles of 0–4°, however, the "best" mean friction angles were δ=15° and 4° for initially non-fluidized and fluidized flows, respectively.

The ratios of the runout of flows on rough (r_r) and smooth (r_s) substrates are represented in Fig. 6. The ratio r_r/r_s increased with the initial column height (i.e., volume) and initial fluidization. For all types of experiments, r_r/r_s increased up to ~1.8–2.2 at low angles <6° then was approximately constant at angles up to 12° and finally decreased down to <1 for a slope of 20°. Data could not be reported at angles >14° for initially fluidized flows as the runout exceeded the channel length. Note that for flows over a rough substrate, the runout considered was either (i) the well-defined distal limit of the deposit determined from observation of flow particles in the substrate interstices (Fig. 6a) or (ii) the maximum extent of the flows observed on videos, which could be several centimeters longer than the observed deposit and whose particles formed a deposit that was too thin to be seen (Fig. 6b). However, both sets of data show similar trends.

Flow front kinematics

Flow front kinematics and velocities are presented in Figs. 7 and 8 for different slope angles. The flows propagated in three successive phases: acceleration, constant velocity, and deceleration, in agreement with trends reported in earlier works on horizontal substrates (e.g., Chédeville and Roche 2014). When the channel base was rough, the relative duration of the final phase (deceleration) increased considerably with the roughness, as the flows were (partially) autofluidized. In consequence, the frontal part of the deposit was greatly elongated compared to that of flows on a smooth substrate.

In the present study, both the flow duration and maximum front velocity increased with the slope angle at given initial conditions (Figs. 7 and 8). For flows over a smooth substrate, the last deceleration phase notably increased with inclination. When the slope was steep enough (~12° for initially fluidized flows and 16° for non-fluidized flows), late-stage mass movement at the free surface of the flow overtook the distal limit of the already deposited material, thus increasing the runout by up to several tens of centimeters. When the substrate was rough, the duration of the acceleration and constant velocity phases increased with the slope angle, whereas the duration of the deceleration phase did not increase despite the higher maximum velocities. As a consequence, the total flow duration increased much less with slope angle compared to what was observed for a smooth substrate. Late-stage mass movement as described above was weak and occurred only near the reservoir.

Flow front morphology

Detailed views of the flow front at different initial conditions are reported in Fig. 9. Flows over a smooth substrate had a thin head whose free surface was at a shallow angle with respect to the substrate and whose base was in direct contact with the

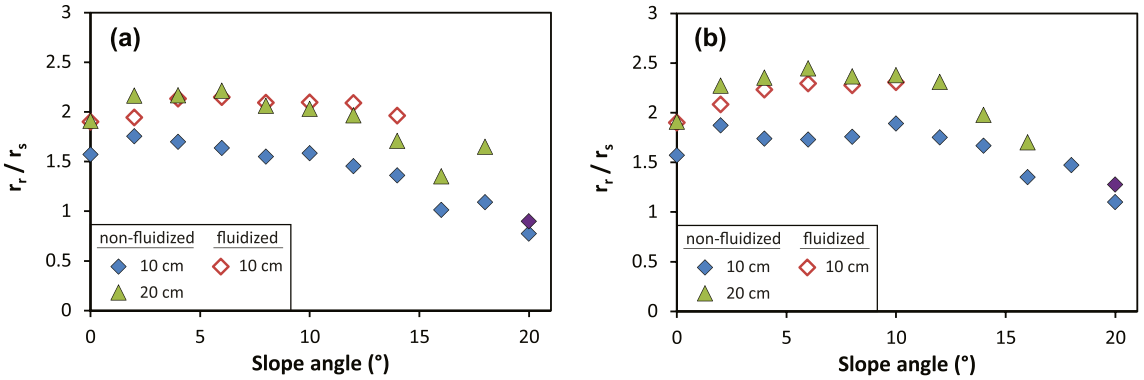

Fig. 6 Ratios of runout distance of flows on 3-mm rough substrate (r_r) over that of flows on a smooth substrate (r_s) for initial column heights of 10 and 20 cm. Runout for a rough substrate was either the distal limit of **a** the deposit observed directly in the channel or **b** the flow visible on video. The purple diamond at 20° corresponds to the runout ratio where late-stage motion overtaking the flow front on a smooth substrate was not taken into account

latter, except at high slope angles (25–30°) where a slight over-elevation of the foremost part could temporarily occur (Fig. 9f). We did not observe any "plunging breakers" that could entrain ambient air, as described by Bareschino et al. (2008) for instance. The head of flows over a rough substrate slid over the glued beads at all angles investigated, and particles settled into the interstices (Fig. 9a–d; see Chédeville and Roche (2014) for a detailed description of flows over a horizontal substrate). Transient front instabilities observed at the foremost part of the flow probably resulted from collisions of the particles with the substrate beads, but, as for a smooth substrate, we did not observe any "plunging breakers."

Sedimentation and deposit reworking

At slope angles of 25 and 30°, the flows left no deposit in the channel at any configuration. During propagation, however, we observed the formation of a thin basal deposit (<5 mm at 80 cm from the gate) that first aggraded and was subsequently eroded slowly by the material flowing above once both flow height (Fig. 10) and velocity had much decreased. This phenomenon was observed in all cases except for initially non-fluidized flows over a smooth substrate. Note that for a rough substrate, deposition occurred sooner after passage of the flow front and was slower compared to a smooth substrate. At an

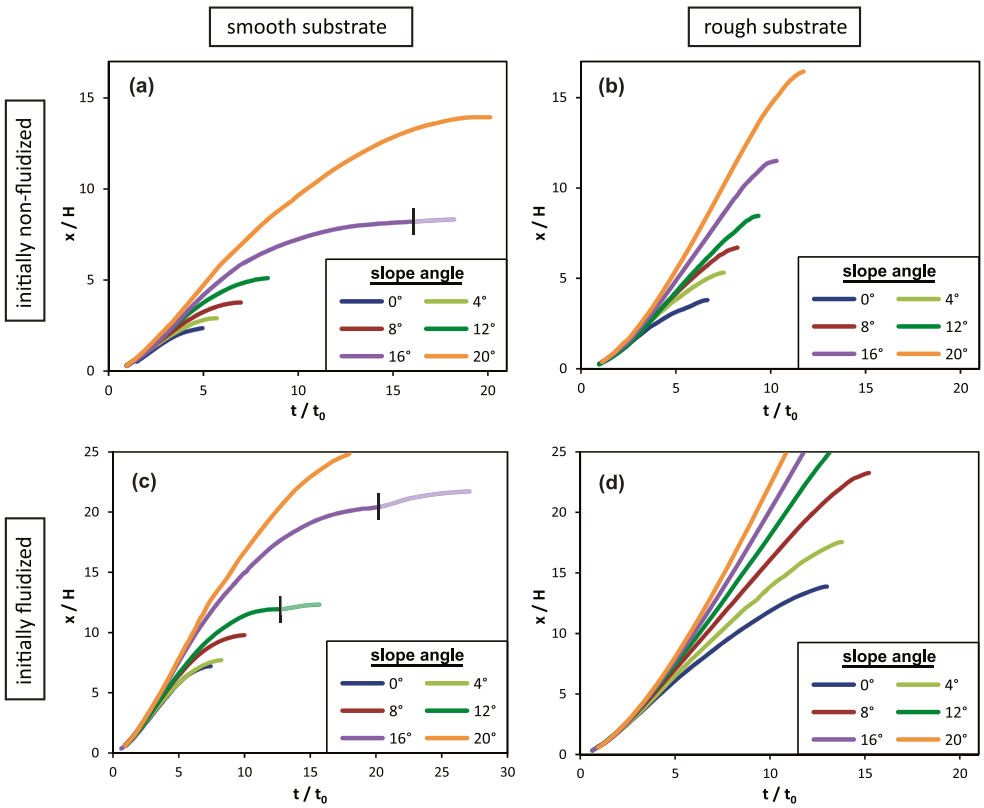

Fig. 7 Normalized flow runout, x/H, as a function of normalized time t/t_0, with $t_0=(H/g)^{1/2}$ at various slope angles for initially non-fluidized flows over **a** a smooth substrate and **b** a rough substrate, and initially fluidized flows over **c** a smooth and **d** a rough substrate. Measurements of the front position were made at time intervals of t/t_0~0.16 s. *Vertical black lines* for some high slope angle data indicate the front being overtaken by a late-stage motion at the upper free surface of the flow. Some curves are truncated as flows exceeded the channel length

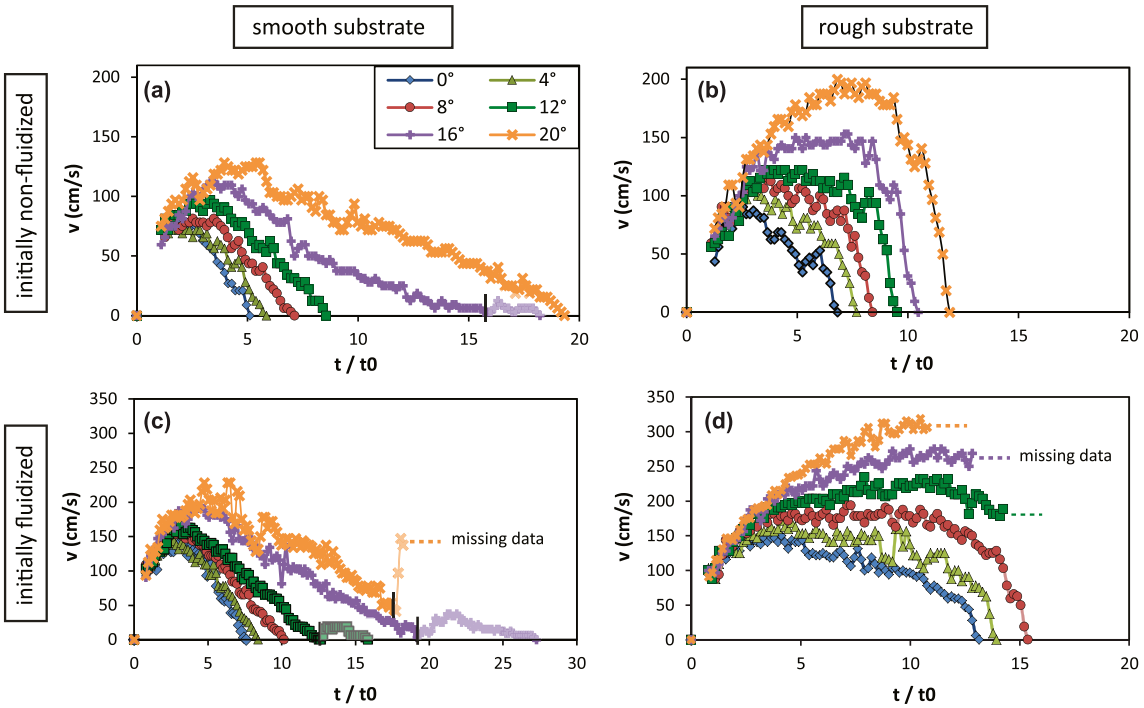

Fig. 8 Flow front velocity as a function of normalized time (t/t_0, see Fig. 7) for slope angles of 0 to 20° and for initially non-fluidized flows propagating over **a** a smooth or **b** a rough substrate, and initially fluidized flows propagating over **c** a smooth or **d** a rough substrate (same legend for all graphs). *Vertical black lines* for some high slope angle data indicate the front being overtaken by a late-stage motion of particles at the upper free surface of the flow. Some curves are truncated because flows exceeded the channel length

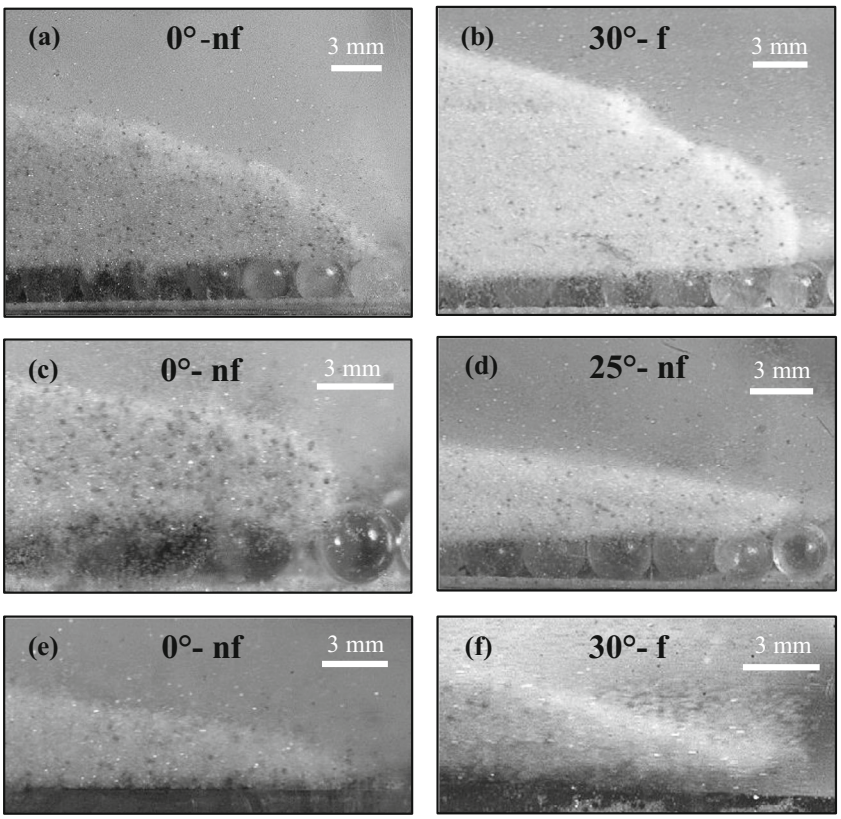

Fig. 9 Detailed views of the flow front for various configurations. **a** Fluidized (*f*) flow, rough substrate at 8°. **b** Fluidized flow, rough substrate at 30°. **c** Non-fluidized flow (*nf*), rough substrate at 0°. **d** Non-fluidized flow, rough substrate at 25°. **e** Non-fluidized flow, smooth substrate at 0°. **f** Fluidized flow, smooth substrate at 30°. Snapshots were taken at 80 cm (**a**, **b**, **d**, and **f**), 45 cm (**c**), or 30 cm (**e**) from the reservoir

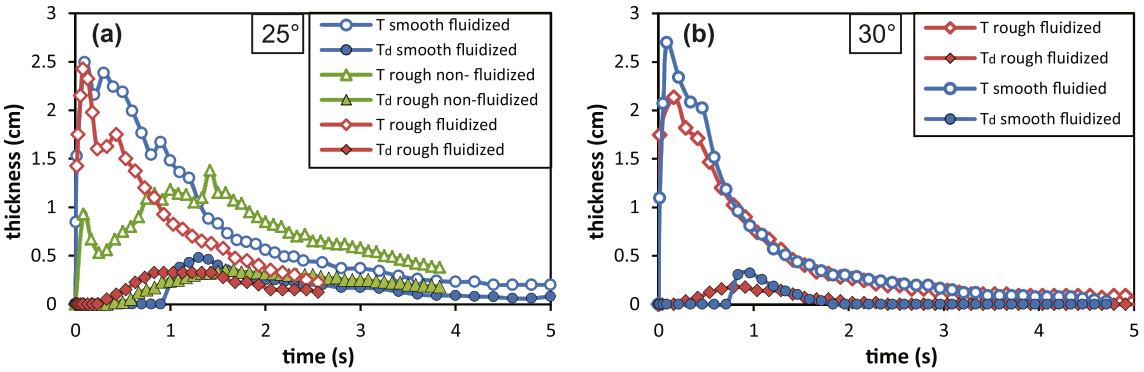

Fig. 10 Thickness of the basal deposit, T_d, and total thickness (flow + deposit), T, as a function of time at 80 cm from the gate and for inclinations of **a** 25° and **b** 30°. Some data are not represented for all flow durations because of difficulties in distinguishing the lower flow boundary

inclination of 30°, the maximum thickness of the deposit was smaller and its erosion was much faster than at 25°.

Discussion

Autofluidization

One of the most important results of our study is that, when initially non-fluidized flows propagated over a rough substrate, high pore pressure (P/P_L>0.75) was measured at all slope angles (0–30°) and at most sensor locations (50–150 cm from the reservoir) investigated. This suggests that the autofluidization mechanism evidenced by Chédeville and Roche (2014) for flows on a horizontal rough substrate was also effective at high slope angles. Though the amplitude of pore pressure signals on inclined surfaces was similar to that in the horizontal configuration, the duration of the signals, which corresponded to the flow length affected by overpressure, increased with the slope angle for a given travel distance (Fig. 4). This could result from a higher flow velocity and lower settling rate that increased the total filling time of the interstices by the flow particles, thus increasing the flow length affected by autofluidization. This was confirmed by video measurements that show that the filling time of the interstices increased from ~0.11 to ~0.21 s when the slope angle increased from 0 to 30°.

Another important result is the absence of overpressure in initially non-fluidized flows propagating over a smooth substrate, even at a slope angle up to 30°. This implies that, in our configuration involving flows at almost maximum particle concentration, autofluidization was not possible or negligible. This contrasts with the experiments of Bareschino et al. (2008) that involved a rotating drum and in which fine particles (glass beads or FCC) were autofluidized. In their study, autofluidization was the result of successive "plunging breakers" that incorporated ambient air at the flow front. At sufficiently high flow velocity (>2.5 m/s), efficient air percolation through the granular mass caused the fine-grained material to acquire a frictionless behavior. In our experiments, no similar front instabilities were observed although the maximum front velocities were higher (up to 5 m/s at an inclination of 30°) than those in the rotating drum experiments. It is possible that the plunging breakers reported by Bareschino et al. (2008) were the consequence of their experimental configuration, as the granular material was elevated at a flow rear by the rotating drum before propagating on very steep flow surfaces towards the front.

Influence of slope angle on flow dynamics

The variation of the flow runout with slope angle <16° for our initially non-fluidized flows over a smooth substrate is well described by the scaling law of Mangeney et al. (2010) and Farin et al. (2014), which means that runout was essentially controlled by the initial column height. At angles >16°, this scaling law overestimated the runout, particularly when late-stage motion was not considered (Fig. 5a). Farin et al. (2014) reported similar results for experiments on steeply inclined rough substrates and proposed that runout was also controlled by the volume released. The main difference with their study was the lower effective friction angle in our experiments (23° against 27°), probably due to the different sizes of the flow particles (d=0.08 mm against d=0.70 mm) and the nature of the substrate we used (smooth Plexiglas against glued glass beads), as the nature of the flow particles (glass beads) and channel walls (Plexiglas) were identical for both studies. Though scaling with a mean low effective friction angle is possible for initially fluidized flows at a given slope angle (see Roche et al. (2011) for horizontal substrate), our results show that it is not applicable for a range of slope angles. This conclusion also applies to our initially non-fluidized flows on rough substrates that were partially autofluidized during propagation and whose emplacement was controlled by a mean friction lower than that of the

non-fluidized material. The ratio of the flow runout on the rough substrate over that on the smooth plane did not vary much (~1.8–2.2) at slope angles up to 10–12°, above which this ratio decreased significantly. This shows that the effect of runout increase due to substrate roughness was reduced at high inclinations, which could be the consequence of several mechanisms: (i) the autofluidization became less efficient at steeper slopes, but strong overpressure signals suggest this was not the case; (ii) the continuous sedimentation of the flow particles in the substrate interstices reduced the mass of the flow whose head (the flow portion with a basal slip condition) ran out of material; (iii) the increase of collision intensity between the flow particles and substrate beads, as the flow velocity increased with the slope angle, could dissipate more flow energy than for a smooth substrate.

Kinematic data reveal that the presence of a rough substrate caused a larger increase of the maximum flow front velocity and of the duration of the acceleration and constant velocity phases with an increasing slope angle compared to a smooth substrate (Fig. 8). Nevertheless, the deceleration phase, which seemed to start only when the flow head thickness had much decreased (<2–3 mm), became abrupt (Fig. 8b, d) and its duration, notably for initially non-fluidized flows, did not vary much ($2.5<t/t_0<3.5$) as the slope angle increased, whereas it was drastically extended for flows on a smooth substrate (t/t_0 varied from 2.5 to 13.5 at inclinations of 0 and 20°, respectively). Rowley et al. (2014) showed that experimental flows fluidized by a continuous air flux along the flow base did not stop even on a horizontal substrate. In our experiments, however, only the flow head was autofluidized through settling of the particles in the substrate interstices and the resulting mass loss could have caused a rapid flow deceleration when, eventually, the flow head became too thin to sustain motion. Increasing the substrate roughness could enlarge the flow portion affected by the fluidization mechanism but, in the same time, could increase the volume of flow particles lost by settling into the interstices. Furthermore, experiments of Chédeville and Roche (2014) on a horizontal substrate showed that when the roughness was too high ($D_0>0.3$–0.6 mm), its positive influence on the runout started to decrease.

Implication for pyroclastic flows

This work shows that the autofluidization mechanism found by Chédeville and Roche (2014) for horizontal substrates can also be efficient at high slope angles (at least 30°). This suggests that, in nature, this mechanism could occur during the whole propagation of pyroclastic flows, from the steep flanks of volcanoes to the distal more gentle slopes.

Air ingestion at the flow front was proposed by McTaggart (1960) and Wilson (1980) as a possible mechanism for the fluidization of pyroclastic flows. This was mainly because the flow head morphology was believed to be similar to that of fluid gravity currents in Boussinesq conditions (i.e., with a low density difference with the surrounding fluid) for which no-slip condition at the lower boundary caused a convex-shaped head with an elevated nose beneath which the surrounding fluid could be ingested (Allen 1971; Simpson 1972, 1986, 1997). In our experiments, however, velocity at the lower boundary was not zero as the flow base slid over the substrate, as commonly observed for granular flows (Artoni et al. 2009). This is probably the main reason why we did not observe a long-lived elevated nose that would have favored basal air incorporation. Note also that mixing with ambient air at the flow upper surface resulting from Kelvin-Helmholtz instabilities (e.g., Andrews and Manga 2012; Andrews 2014) was impossible because of the large density difference between the flow and the surrounding medium, in contrast to Boussinesq gravity currents. In nature, however, pyroclastic flows may be less dense than in our experiments and are commonly faster. For these reasons, we do not rule out that conditions of air incorporation at flow boundaries could be reached at least locally. Moreover, although we did not observe "plunging breakers" (c.f. Bareschino et al. 2008) that would also have permitted air ingestion in our experiments, such phenomena may occur in nature if a flow passes a break in slope or an obstacle.

Reworking of a freshly deposited material by the upper flowing part at a high inclination (25–30°) in our experiments may have implications for some pyroclastic flow deposit sequences. During some moderate to large ignimbrite-forming eruptions, waxing and waning phases are thought to alternate (Branney and Kokelaar 2002; Brown and Branney 2013; Williams et al. 2013; Brand et al. 2014), which could lead to successive episodes of deposition and erosion (Brown and Branney 2004) and could render the deposit architecture difficult to decipher. In our experiments, the flows first formed a basal deposit that was then progressively eroded as the flow thickness and velocity decreased. The recent study of Lucas et al. (2014) suggests that the basal friction of geophysical granular flows can vary inversely with their velocity; accordingly, onset of erosion at decreasing velocity in our experiments is compatible with increasing friction at the base of the flowing mass. Another possibility is that basal friction increased with time as the granular material defluidized progressively. We stress that our results are very preliminary and that further work is required to better characterize conditions of deposit remobilization, including particularly the critical flow velocity and substrate slope angle.

Conclusion

Our experiments on flows of fine particles over smooth or rough substrates inclined up to 30° have revealed that

(1) The autofluidization mechanism of fines-rich pyroclastic flows evidenced by experiments of Chédeville and Roche (2014) and caused by air evacuation from the interstices of a rough substrate into which the flow particles settled occurred at all slope angles investigated (0–30°). In contrast, autofluidization was not generated in case of a smooth substrate.
(2) Flow front instabilities that may favor incorporation of the ambient air such as plunging breakers or those typical of fluid gravity currents were never observed, even when the flows propagated on steep slopes (30°). We acknowledge, however, that such instabilities could occur in less dense and/or faster pyroclastic flows or if these encounter a break in slope or an obstacle.
(3) The runout distance of flows on the rough substrate was about twice as that on the smooth incline for slope angles up to 10–12°. For steeper slopes, strong deceleration of the flows on a rough substrate led to relative shorter runout distances, which became close to those for a smooth substrate at a slope angle of 20°. This could result from reduction of the flowing mass, as particles sedimented into the interstices, and/or increase of the energy dissipation through collisions on the rough substrate.
(4) At a slope angle close to the repose angle of the flow material, a deposit first formed at the flow base and was then reworked by the material still in motion above it. The cause of this phenomenon is unclear. It appears that erosion occurred once the flow thickness and/or velocity were low enough, and in this regard, lower velocities of the flowing mass might have caused higher frictional stresses on the basal deposit (Lucas et al. 2014). Further investigation is required to characterize in particular critical normal/shear stress ratio, flow velocity, and slope angle at which erosion occurs. Such a reworking mechanism in pyroclastic flows could create deposits that would not necessarily record the entire flow history and that could locally display complex architecture with remobilized material deposited downstream onto younger products.

Acknowledgments We are grateful to Greg Valentine and David Jessop for the interesting discussions and comments that helped to improve the manuscript. We thank the associate editor Gert Lube, Ben Andrews, and Eric Bréard for the careful and constructive reviews. This work was financed by the Laboratoire Mixte International SVAN of Institut de Recherche pour le Développement (IRD, France) and by the French Government Laboratory of Excellence initiative n°ANR-10-LABX-0006, the Région Auvergne and the European Regional Development Fund. This is Laboratory of Excellence ClerVolc contribution number 169.

References

Allen JRL (1971) Mixing at turbidity current heads, and its geological implications. J Sediment Petrol 41:97–113

Andrews BJ (2014) Dispersal and air entrainment in unconfined dilute pyroclastic density currents. Bull Volcanol 76:852, doi: 8 10.1007/s00445-00014-00852-00444

Andrews BJ, Manga M (2012) Experimental study of turbulence, sedimentation, and coignimbrite mass partitioning in dilute pyroclastic density currents. J Volcanol Geotherm Res 225–226:30–44. doi:10.1016/j.jvolgeores.2012.1002.1011

Artoni R, Santomaso AC, Canu P (2009) Effective boundary conditions for dense granular flows. Phys Rev E 79:031304. doi:10.1103/PhysRevE.79.031304

Bareschino P, Lirer L, Marzocchella A, Petrosino P, Salatino P (2008) Self-fluidization of subaerial rapid granular flows. Powder Technol 182:323–333. doi:10.1016/j.powtec.2007.12.010

Bernard J, Kelfoun K, Le Pennec J-L, Vallejo Vargas S (2014) Pyroclastic flow erosion and bulking processes: comparing field-based vs. modeling results at Tungurahua volcano, Ecuador. Bull Volcanol 76:858. doi:10.1007/s00445-014-0858-y

Brand BD, Mackaman-Lofland C, Pollock NM, Bendaña S, Dawson B, Wichgers P (2014) Dynamics of pyroclastic density currents: conditions that promote substrate erosion and self-channelization—Mount St Helens, Washington (USA). J Volcanol Geotherm Res 276:189–214. doi:10.1016/j.jvolgeores.2014.01.007

Branney MJ, Kokelaar BP (2002) Pyroclastic density currents and the sedimentation of ignimbrites. Geol Soc Lond Mem 27

Brown RJ, Branney MJ (2004) Bypassing and diachronous deposition from density currents: evidence from a giant regressive bed form in the Poris ignimbrite, Tenerife, Canary Islands. Geology 32:445–448. doi:10.1130/G20188.1

Brown RJ, Branney MJ (2013) Internal flow variations and diachronous sedimentation within extensive, sustained, density-stratified pyroclastic density currents flowing down gentle slopes, as revealed by the internal architectures of ignimbrites on Tenerife. Bull Volcanol 75:727. doi:10.1007/s00445-013-0727-0

Calder ES, Sparks RSJ, Gardeweg MC (2000) Erosion, transport and segregation of pumice and lithic clasts in pyroclastic flows inferred from ignimbrite at Lascar Volcano, Chile. J Volcanol Geotherm Res 104:201–235

Chédeville C, Roche O (2014) Autofluidization of pyroclastic flows propagating on rough substrates as shown by laboratory experiments. J Geophys Res 119:1764–1776. doi:10.1002/2013JB010554

Druitt TH (1998) Pyroclastic density currents. Geol Soc Lond Spec Publ 145–182

Druitt TH, Avard G, Bruni G, Lettieri P, Maez F (2007) Gas retention in fine-grained pyroclastic flow materials at high temperatures. Bull Volcanol 69:881–901. doi:10.1007/s00445-007-0116-7

Farin M, Mangeney A, Roche O (2014) Fundamental changes of granular flow dynamics, deposition, and erosion processes at high slope angles: insights from laboratory experiments. J Geophys Res 119:504–532. doi:10.1002/2013JF002750

Fisher R, Orsi G, Ort M, Heiken G (1993) Mobility of a large-volume pyroclastic flow—emplacement of the Campanian ignimbrite, Italy. J Volcanol Geotherm Res 56:205–220

GDR MiDi (2004) On dense granular flows. Eur Phys J E 14:341–365. doi:10.1140/epje/i2003-10153-0

Giordano G (1998) The effect of paleotopography on lithic distribution and facies associations of small volume ignimbrites: the WTT Cupa (Roccamonfina volcano, Italy). J Volcanol Geotherm Res 87:255–273

Girolami L, Druitt TH, Roche O, Khrabrykh Z (2008) Propagation and hindered settling of laboratory ash flows. J Geophys Res 113: B02202. doi:10.1029/2007JB005074

Iverson RM (1997) The physics of debris flows. Rev Geophys 35:245–296

Lube G, Cronin SJ, Platz T, Freundt A, Procter JN, Henderson C, Sheridan MF (2007) Flow and deposition of pyroclastic granular flows: a type example from the 1975 Ngauruhoe eruption, New Zealand. J Volcanol Geotherm Res 161:165–186. doi:10.1016/j.jvolgeores.2006.12.003

Lube G, Huppert HE, Sparks RSJ, Freundt A (2011) Granular column collapses down rough, inclined channels. J Fluid Mech 675:347–368. doi:10.1017/jfm.2011.21

Lucas A, Mangeney A (2007) Mobility and topographic effects for large Valles Marineris landslides on Mars. Geophys Res Lett 34:L10201. doi:10.1029/2007GL029835

Lucas A, Mangeney A, Ampuero JP (2014) Frictional velocity-weakening in landslides on Earth and on other planetary bodies. Nat Commun 5:3417. doi:10.1038/ncomms4417

Mangeney A, Bouchut F, Thomas N, Vilotte JP, Bristeau MO (2007) Numerical modeling of self-channeling granular flows and of their levee-channel deposit. J Geophys Res 112:F02017. doi:02010.01029/02006JF000469

Mangeney A, Roche O, Hungr O, Mangold N, Faccanoni G, Lucas A (2010) Erosion and mobility in granular collapse over sloping beds. J Geophys Res 115:1–21. doi:10.1029/2009JF001462

McTaggart K (1960) The mobility of nuées ardentes. Am J Sci 258:369–382

Montserrat S, Tamburrino A, Roche O, Niño Y (2012) Pore fluid pressure diffusion in defluidizing granular columns. J Geophys Res 117:F02034. doi:10.1029/2011JF002164

Rhodes MJ (1998) Introduction to particle technology. John Wiley, Chichester

Roche O (2012) Depositional processes and gas pore pressure in pyroclastic flows: an experimental perspective. Bull Volcanol 74:1807–1820. doi:10.1007/s00445-012-0639-4

Roche O, Gilbertson MA, Phillips JC, Sparks RSJ (2006) The influence of particle size on the flow of initially fluidized powders. Powder Technol 166:167–174. doi:10.1016/j.powtec.2006.05.010

Roche O, Montserrat S, Niño Y, Tamburrino A (2010) Pore fluid pressure and internal kinematics of gravitational laboratory air-particle flows: insights into the emplacement dynamics of pyroclastic flows. J Geophys Res 115:B09206. doi:10.1029/2009JB007133

Roche O, Attali M, Mangeney A, Lucas A (2011) On the run-out distance of geophysical gravitational flows: insight from fluidized granular collapse experiments. Earth Planet Sci Lett 311:375–385. doi:10.1016/j.epsl.2011.09.023

Roche O, Niño Y, Mangeney A, Brand B, Pollock N, Valentine G (2013) Dynamic pore pressure variations induce substrate erosion by pyroclastic flows. Geology 41:1107–1110. doi:10.1130/G34668.1

Rowley PJ, Roche O, Druitt TH, Cas R (2014) Experimental study of dense pyroclastic density currents using sustained, gas-fluidized granular flows. Bull Volcanol 76:855. doi:10.1007/s00445-014-0855-1

Simpson JE (1972) Effects of the lower boundary on the head of a gravity current. J Fluid Mech 53:759. doi:10.1017/S0022112072000461

Simpson JE (1986) Mixing at the front of a gravity current. Acta Mech 63:245–253. doi:10.1007/BF01182551

Simpson JE (1997) Gravity currents in the environment and the laboratory. Cambridge University Press, Cambridge

Sparks RSJ (1976) Grain size variations in ignimbrites and implications for the transport of pyroclastic flows. Sedimentology 23:147–188

Sparks RSJ, Gardeweg M, Calder E, Matthews SJ (1997) Erosion by pyroclastic flows on Lascar Volcano. Chile. Bull Volcanol 58:557–565

Valentine G, Buesch D, Fisher R (1989) Basal layered deposits of the peach springs tuff, northwestern Arizona, USA. Bull Volcanol 51:395–414

Williams R, Branney MJ, Barry TL (2013) Temporal and spatial evolution of a waxing then waning catastrophic density current revealed by chemical mapping. Geology 42:107–110. doi:10.1130/G34830.1

Wilson C (1980) The role of fluidization in the emplacement of pyroclastic flows: an experimental approach. J Volcanol Geotherm Res 8:231–249

Wilson C, Houghton B, Kamp PJJ, McWilliams MO (1995) An exceptionally widespread ignimbrite with implications for pyroclastic flow emplacement. Nature 378:605–607

Woods AW, Bursik M, Kurbatov A (1998) The interaction of ash flows with ridges. Bull Volcanol 60:38–51